

# Mapping H<sub>2</sub> Excitation and Mass across NGC 5194 with the Spitzer Infrared Spectrograph

Gregory Brunner<sup>1,2</sup>

Department of Physics and Astronomy, Rice University,  
Houston, TX 77005

gbrunner@ipac.caltech.edu, gbrunner@rice.edu

Kartik Sheth<sup>3</sup>, Lee Armus<sup>3</sup>, and George Helou<sup>3</sup>

Spitzer Science Center, Pasadena, CA 91125

Eva Schinnerer<sup>4</sup>

Max-Planck-Institüt für Astronomie, Heidelberg, Germany

and

Stuart Vogel<sup>5</sup> and Mark Wolfire<sup>5</sup>

Department of Astronomy, University of Maryland, College Park, MD 20741

Received \_\_\_\_\_; accepted \_\_\_\_\_

---

<sup>1</sup>Department of Physics and Astronomy, Rice University, Houston, TX 77005

<sup>2</sup>Visiting Graduate Student Fellow, Spitzer Science Center, Caltech, Pasadena, CA 91125

<sup>3</sup>Spitzer Science Center, Caltech, Pasadena, CA 91125

<sup>4</sup>Max-Planck-Institüt für Astronomie, Heidelberg, Germany

<sup>5</sup>Department of Astronomy, University of Maryland, College Park, MD 20741

## ABSTRACT

We have mapped H<sub>2</sub> pure rotational line emission for the H<sub>2</sub> S(0) - H<sub>2</sub> S(5) lines over a strip across NGC 5194 using the *Spitzer Space Telescope* Infrared Spectrograph low resolution modules. The H<sub>2</sub> line intensity maps reveal differences in the molecular gas morphology of NGC 5194. We use the H<sub>2</sub> maps to model the H<sub>2</sub> excitation-temperature and mass across the galaxy. We find that within our beam, H<sub>2</sub> exists in a continuous distribution of temperatures across the galaxy. We distinguish between a warm (T = 100 - 300 K) H<sub>2</sub> mass phase traced by the low  $J$  lines and a hot (T = 400 - 1000 K) H<sub>2</sub> mass phase traced by higher  $J$  lines in order to map the excitation-temperature and mass of the warm and hot H<sub>2</sub> phases. We find that the warm H<sub>2</sub> excitation-temperature is highest in the nuclear region (192 K) and is lower within the spiral arms (150 - 170 K). The hot H<sub>2</sub> excitation-temperature is lowest in the inner spiral arms (500 - 550 K), where the greatest hot H<sub>2</sub> masses are found. The warm-to-hot H<sub>2</sub> mass ratio is not constant across the galaxy indicating a different origin and different primary excitation mechanisms to the warm H<sub>2</sub> mass phase (and low  $J$  line emission) and hot H<sub>2</sub> mass phase (and higher  $J$  line emission). We investigate the origin of the H<sub>2</sub> emission by comparing the location and magnitude of H<sub>2</sub> emission and mass to photodissociation regions (traced by CO ( $J = 1 - 0$ ) emission), shock-excited [O IV](25.89  $\mu\text{m}$ ) emission, and X-ray dissociation regions from *Chandra* observations. We find that within the spiral arms, the H<sub>2</sub> mass correlates with the CO ( $J = 1 - 0$ ) emission; although, we see offsets in the location of the peaks in H<sub>2</sub> mass and CO intensity. Comparing H<sub>2</sub> line intensity to CO intensity reveals that within the spiral arms, pure rotational H<sub>2</sub> line emission is generally cospatial with CO emission indicating that the pure rotational H<sub>2</sub> line emission is connected with the surface layers of dense molecular clouds

associated with star-forming regions. Within the nuclear region of NGC 5194, the hot H<sub>2</sub> phase correlates with [O IV](25.89  $\mu\text{m}$ ) emission and X-ray emission while the warm H<sub>2</sub> does not. Comparison between X-ray emission and H<sub>2</sub> line emission shows that the H<sub>2</sub> morphology is correlated with X-rays. These comparisons reveal that shocks and X-rays are responsible for exciting the hot H<sub>2</sub> phase in the nuclear region of NGC 5194, though the contribution of shocks and X-rays cannot be distinguished from each other due to the low (10''.2) resolution of the [O IV](25.89  $\mu\text{m}$ ) and hot H<sub>2</sub> mass maps.

*Subject headings:* galaxies: ISM — galaxies: H<sub>2</sub> — galaxies: individual(NGC 5194)

## 1. Introduction

Star formation and galactic evolution are inherently connected with the molecular gas within a galaxy. In the Milky Way, all star formation occurs in molecular clouds (Blitz 1995); although, not all molecular clouds are actively forming stars. In galaxies, star formation is triggered whenever the molecular gas surface density is enhanced, for example, by a spiral density wave (Vogel et al. 1988), by increased pressure in galactic nuclei (Young and Devereux 1991), due to the hydrodynamic shock along the leading edge of bars, and in the transition region at the ends of bars (Sheth et al. 2000, Kenney and Lord 1991). Although the connection between star formation and molecular gas is well-established, the exact mechanisms for initiating, controlling, and inhibiting star formation are not well-understood.

Prior to the advent of space-born infrared observatories such as the Infrared Space Observatory (ISO) and the Spitzer Space Telescope (*Spitzer*), much of our knowledge of the conditions of the molecular hydrogen (the most abundant molecule in the interstellar medium (ISM)) in galaxies came from studies of CO emission and rotational-vibrational H<sub>2</sub> line emission in the near-infrared. CO rotational line emission directly traces the mass of the coldest (T = 5 - 100 K) H<sub>2</sub> while the near-infrared H<sub>2</sub> line emission traces the hot (T ≥ 1000 K) H<sub>2</sub>. The CO (J = 1 - 0) line at 2.6 mm has served as a means to infer the mass of the coldest (T = 5 - 10 K) H<sub>2</sub>, which, owing to a lack of a permanent dipole moment, is undetectable in cold, dense molecular clouds. Studies of CO in galaxies often seek to measure the cold (T = 5 - 100 K) H<sub>2</sub> mass by invoking an *X* factor to convert directly from CO intensity to H<sub>2</sub> mass (Young and Scoville 1991). Studies of the near-infrared H<sub>2</sub> rovibrational emission have utilized ground-based telescopes equipped with either narrow-band H<sub>2</sub> filters or a Fabry-Perot spectrometer. While some studies have had success in resolving rovibrational H<sub>2</sub> emission lines such as H<sub>2</sub>(2-1)S(1)(2.25 μm) and

$\text{H}_2(1-0)\text{S}(1)(2.12 \mu\text{m})$  in the nuclear regions of galaxies (Moorwood and Oliva 1990, Davies et al. 2003), resolving these lines across galaxies has been hindered due to the low surface brightness of the rovibrational lines (Pak et al. 2004).

The Whirlpool galaxy (M51a, NGC 5194) is a nearby, face-on galaxy that contains massive amounts of molecular gas as inferred from CO observations. At a distance of 8.2 Mpc, its proximity, orientation, and morphology make it an ideal target for studies of the ISM across distinct dynamical, chemical, and physical environments in a galaxy. Studies of the molecular gas within NGC 5194 have revealed giant molecular associations (GMAs) along the spiral arms (Aalto et al. 1999), massive amounts of  $\text{H}_2$  ( $\sim 1 \times 10^7 \text{ M}_\odot$ ) fueling the nuclear AGN (Scoville et al. 1998), and star-formation synchronized by a spiral density wave (Vogel et al. 1988). In addition to being well-studied in CO, NGC 5194 has been extensively studied in X-rays (Palumbo et al. 1985, Terashima et al. 2001); UV, optical (Scoville et al. 2001), and IR (Calzetti et al. 2005); submillimeter (Matsushita et al. 2004); millimeter (Helfer and Blitz 1997); and radio wavelengths (Murphy et al. 2005). The proximity, orientation, and grand-design structure of NGC 5194 coupled with the wealth of observations and knowledge associated with the galaxy have inspired astronomers to refer to it as a *Rosetta Stone* for galaxy evolution (Scoville and Young, 1983).

The *Spitzer* Infrared Spectrograph (IRS) (Houck et al. 2004) is a powerful tool for observing the molecular gas within galaxies and thus deciphering the evolution of NGC 5194. The *Spitzer* IRS low resolution modules cover 5 - 38  $\mu\text{m}$  (short-low, SL, 5 - 14  $\mu\text{m}$ ; long-low, LL, 14 - 38  $\mu\text{m}$ ) giving observers access to the lowest pure rotational  $\text{H}_2$  lines. These lines trace the warm ( $T = 100 - 1000 \text{ K}$ ) molecular gas and are important diagnostics of the ISM allowing for the modeling of the  $\text{H}_2$  excitation-temperature, mass, and ortho-to-para ratio. By understanding the pure rotational  $\text{H}_2$  line emission from a galaxy, constraints can be placed on the energy injection mechanisms (i.e. radiative heating,

shocks, turbulence) that heat the warm molecular gas phase in the ISM.

In this paper, we present spatially resolved observations of the H<sub>2</sub> rotational lines across a radial strip of NGC 5194. Using the *Spitzer* IRS, we have spectrally mapped a radial strip (406'' x 56'' in the LL and 324'' x 57'' in the SL) across NGC 5194 in order to understand the conditions of the warm (T = 100 - 1000 K) molecular ISM across dynamically distinct environments. From the spatially resolved IRS low resolution spectra, emission from the six lowest pure rotational transitions of H<sub>2</sub> (the H<sub>2</sub>(0-0)S(0) (28.22  $\mu$ m), H<sub>2</sub>(0-0)S(1) (17.04  $\mu$ m), H<sub>2</sub>(0-0)S(2) (12.28  $\mu$ m), H<sub>2</sub>(0-0)S(3) (9.66  $\mu$ m), H<sub>2</sub>(0-0)S(4) (8.02  $\mu$ m), and H<sub>2</sub>(0-0)S(5) (6.91  $\mu$ m) lines) is mapped across the NGC 5194 strip (§3.1). These maps represent measurements of extinction-corrected line intensities across NGC 5194. The maps are used to model the spatial variations in the H<sub>2</sub> excitation-temperature and mass across the galaxy (§4.1 and §4.2). We attempt to distinguish the primary excitation mechanism of H<sub>2</sub> (photodissociation by UV photons, shocks, or X-ray dissociation) in various regions across the galaxy by comparing the H<sub>2</sub> distribution to CO (J = 1 - 0) emission (§4.3), [O IV](25.89  $\mu$ m) emission (§4.4), and X-rays (§4.5).

## 2. Observations and Data Reduction

### 2.1. Spectral Data

Spectra were obtained for NGC 5194 using the two low-resolution modules of the Infrared Spectrograph in spectral mapping mode. In spectral mapping mode, we moved the IRS in a series of discrete steps settling at each position before beginning integration. Half slit spacings were used for all integrations. Integration times in the SL and LL were 14.6 s. Each slit position was covered twice. In total, 1,412 spectra were taken in the SL while 100 were taken in the LL (including background observations). SL integrations

were taken perpendicular to the LL integrations in accordance with the SINGS radial strip mapping strategy specified in by Kennicutt et al. (2003). Dedicated off source background observations were taken for the SL observations. Backgrounds for the LL observations were taken from outrigger data collected while the spacecraft was mapping in the adjacent module. Further details on the observation strategy are available on SST’s Leopard for project ID 200138 (PI: K. Sheth).

The spectra were assembled from the basic calibration data into spectral data cubes for each module using CUBISM (Smith et al. 2007, in press). Background subtraction and bad pixel removal was done within CUBISM. The individual IRS spectra were processed using version S14.0 of the Spitzer Science Center pipeline.

In CUBISM, the SL and LL data cubes have resolutions of  $1.85''/\text{pixel}$  and  $5.08''/\text{pixel}$ . The spatial resolution of the data cubes varies as a function of wavelength due to a wavelength dependent point spread function (PSF). Though the pixels are square, the PSF is circular and expands in radius with increasing wavelength. We define the spatial resolution at a given wavelength in the SL and LL data cubes as

$$R_{SL}(\lambda) = 1''.85 \times \lambda/5.2\mu\text{m} \quad (1)$$

and

$$R_{LL}(\lambda) = 5''.08 \times \lambda/14.0\mu\text{m}, \quad (2)$$

respectively, where  $\lambda$  is the wavelength.

Maps of the  $\text{H}_2 \text{ S}(0) - \text{H}_2 \text{ S}(5)$  lines were created with PAHFIT (Smith et al. 2007), a robust mid-infrared spectral fitting routine. PAHFIT decomposes an IRS low resolution spectrum allowing the recovery of the full flux of blended features. This allows the recovery of the full line flux of the  $\text{H}_2$  features, including severely blended lines such as  $\text{H}_2 \text{ S}(1)$ , blended with the  $17.0 \mu\text{m}$  PAH complex (Smith et al. 2004);  $\text{H}_2 \text{ S}(2)$ , blended with  $[\text{Ne II}]$ ( $12.8 \mu\text{m}$ ); and  $\text{H}_2 \text{ S}(5)$ , blended into  $[\text{Ar II}]$ ( $6.9 \mu\text{m}$ ).

In order to run PAHFIT though the SL and LL data cubes, the grid of the SL1 data cube was interpolated to the grid of the SL2 data cube. The data cubes were then concatenated into one SL cube. The same procedure was used to concatenate the LL1 and LL2 data cubes into one LL data cube. In regions where the first order (SL1, LL1) spectra overlapped with the second order (SL2, LL2) spectra, the first order spectra were scaled up to the second order spectra. The concatenated data cubes were then smoothed spatially by a  $3 \times 3$  pixel box to increase the signal to noise ratio of the spectra. Grouping spectra was also done to avoid pixel aliasing, which has the affect of creating a saw-tooth pattern in the continuum (CUBISM User Manual). PAHFIT was then run through both the SL and LL data cubes. The SL and LL data cubes were fit separately.

PAHFIT decomposes every spectrum in both the SL and LL data cubes. In doing so, PAHFIT returns fit parameters to specified features in the spectrum. These parameters include extinction-corrected integrated line intensity, line FWHM, line equivalent width, and uncertainty. The integrated line intensity measurements are extinction-corrected within PAHFIT (see Smith et al. 2007 for the extinction curve). While running PAHFIT through the data cubes, information concerning the position of each spectrum was retained. This allows for the reconstruction of spectral feature (PAH, H<sub>2</sub>, and atomic line) maps from the results of PAHFIT. When using PAHFIT on an entire data cube, maps of every feature specified by PAHFIT were returned. The list of spectral features that PAHFIT measures can be found in Smith et al. (2007). This list can be edited and lines can be easily added or removed from the fit parameters. We have left the line list unchanged. Additionally, the fit to each spectrum was retained and the fit to the continuum was reconstructed from internal PAHFIT functions. From these two data cubes, a residual data cube and a continuum subtracted data cube were created for both the SL and LL data cubes. These data cubes are crucial in determining the consistency of the fitted spectra. For example, to check the accuracy of the map of H<sub>2</sub> S(3) integrated flux, it was compared to the image created from

the continuum subtraction to the SL data cube.

In using PAHFIT, the default values for the temperatures of the starlight and eight thermal dust continuum components were used to fit the continuum. Additionally, the optical depth of the dust extinction at  $9.7\text{ }\mu\text{m}$  and  $18\text{ }\mu\text{m}$  were also fit. This was especially important in recovering an accurate measurement of the  $\text{H}_2\text{ S(3)}$  ( $9.66\text{ }\mu\text{m}$ ) line in the  $9.7\text{ }\mu\text{m}$  silicate absorption trough.

## 2.2. CO Map

The BIMA (Berkely Illinois Maryland Array) CO ( $J = 1 - 0$ ) map was acquired as a part of the BIMA Survey of Nearby Galaxies (SONG) (Regan et al. 2001; Helfer et al. 2003). The CO map was mosaicked from 26 fields. The beam size is  $5''8 \times 5''1$  ( $220\text{ pc} \times 190\text{ pc}$ ), the velocity channel width is  $10\text{ km s}^{-1}$ , and the root-mean-square (rms) noise level is  $61\text{ mJy beam}^{-1}$ .

## 2.3. X-ray Emission

X-ray emission from M51 was observed by the Advanced CCD Imaging Spectrometer (ACIS) on the *Chandra X-Ray Observatory* on 20 June 2000. The total integration time was 14,865 seconds. Further details of the observations are presented in Terashima and Wilson (2001).

### 3. Results

#### 3.1. H<sub>2</sub> Emission Maps

Molecular Hydrogen emission has been detected and mapped across NGC 5194 for the H<sub>2</sub> S(0), H<sub>2</sub> S(1), H<sub>2</sub> S(2), H<sub>2</sub> S(3), H<sub>2</sub> S(4), and H<sub>2</sub> S(5) lines. In Figure 1, maps of the extinction-corrected intensity of the of the H<sub>2</sub> S(0) - H<sub>2</sub> S(5) lines are presented. The H<sub>2</sub> S(0) and H<sub>2</sub> S(1) lines lie in the LL module of the *Spitzer* IRS and the resolution of the maps are 10''.2 and 6''.17, respectively. The rectangular box around the maps represents the 295'' × 51'' region where the LL1 and LL2 strips overlap. The H<sub>2</sub> S(2), H<sub>2</sub> S(3), H<sub>2</sub> S(4), and H<sub>2</sub> S(5) lines lie in the SL module of the *Spitzer* IRS and these maps have spatial resolutions of 4''.37, 3''.44, 2''.85, and 2''.46, respectively. The rectangular box around the maps represents the 324'' × 57'' region where the SL1 and SL2 strips overlap. The differences in resolution between the H<sub>2</sub> maps explains the relative smoothness of H<sub>2</sub> S(0) and H<sub>2</sub> S(1) maps compared to the H<sub>2</sub> S(2) - H<sub>2</sub> S(5) maps. Table 1 lists the resolution of the maps. Note that the orientation of the H<sub>2</sub> S(0) and H<sub>2</sub> S(1) maps is offset from the H<sub>2</sub> S(2) - H<sub>2</sub> S(5) maps due to the gradual roll of the sky over the period of time that the spectra were observed.

The maps of H<sub>2</sub> rotational line intensity reveal remarkable differences in the morphology of NGC 5194 through each line. H<sub>2</sub> S(0) emission is strongest in the northwest spiral arm with much lower levels of emission coming from the nucleus. The H<sub>2</sub> S(1) emission peaks in the nucleus of the galaxy with strong emission in the northwest and southeast spiral arms. The peaks in H<sub>2</sub> S(0) and H<sub>2</sub> S(1) emission within the arms do not align. These offsets are real; they do not result from the difference in resolution between the two maps. H<sub>2</sub> S(0) and H<sub>2</sub> S(1) emission is resolved out to 7 kpc from the nucleus of the galaxy showing that the warm H<sub>2</sub> is detectable at large distances from the central regions of the galaxy.

The higher resolution H<sub>2</sub> S(2) - H<sub>2</sub> S(5) maps also show different morphology to the molecular gas within NGC 5194. The H<sub>2</sub> S(2) map shows the strongest emission in the nuclear region of NGC 5194. The H<sub>2</sub> S(3) line exhibits similar strong emission in the nuclear region; however, there appears to be a bar structure across the nucleus of the galaxy going north-to-south. Again, there are offsets in the peak emission within the spiral arms of NGC 5194. These differences in morphology are real and indicate variations in the excitation-temperature in each region.

We resolve diffuse emission from the H<sub>2</sub> S(4) and H<sub>2</sub> S(5) lines across NGC 5194. These lines are very faint across the disk of the galaxy but both show strong emission from the nuclear region. The H<sub>2</sub> S(5) morphology reveals assymetry in the H<sub>2</sub> emission from the nucleus. The H<sub>2</sub> S(5) emission mimics that of the H<sub>2</sub> S(3) line with extended emission to the north of the nucleus. The H<sub>2</sub> S(4) line shows emission in the nucleus and in the spiral arm to the west. This is notable because the spiral arm to the southwest of the nucleus is very bright in CO and studies have revealed very high molecular gas column densities in the southwest inner spiral arm (Lord and Young 1990). The differences in the H<sub>2</sub> morphology are indicative of variations in the H<sub>2</sub> excitation-temperature across the galaxy.

#### 4. Discussion

##### 4.1. H<sub>2</sub> Excitation-Temperature and Mass across NGC 5194

The pure rotational lines of molecular hydrogen provide a powerful probe of the conditions of the ISM and place constraints on the energy injection processes that excite H<sub>2</sub>. Knowledge of the extinction-corrected intensity of the H<sub>2</sub> S(0) - H<sub>2</sub> S(5) lines allow for the determination of the H<sub>2</sub> excitation-temperature, number density (and consequently mass), and ortho-to-para ration (OPR) (Rigopoulou et al. 2002, Higdon et al. 2006, Neufeld et al.

2006). From the maps of the pure rotational H<sub>2</sub> emission, the excitation-temperature and mass can be modeled across the galaxy.

In order to model the H<sub>2</sub> excitation and mass across the galaxy, the H<sub>2</sub> S(1) - H<sub>2</sub> S(5) maps were smoothed to the resolution of the H<sub>2</sub> S(0) map, 10''.2 (380 pc). The maps were then interpolated to the same spatial grid. Excitation diagrams across the strip were derived from the Boltzman equation in similar form to the Rigopoulou et al. (2002),

$$N_i/N = (g(i)/Z(T_{\text{ex}})) \exp(-T_i/T_{\text{ex}}) \quad (3)$$

where  $g(i)$  is the statistical weight of state  $i$ ,  $Z(T_{\text{ex}})$  is the partition function,  $T_i$  is the energy level of a given state, and  $T_{\text{ex}}$  is the excitation temperature.  $N$  and  $N_i$  are the total column density and the column density of a given state  $i$  and  $N_i$  is determined directly from the measured extinction-corrected flux by

$$N_i = 4\pi \times \text{flux}(i)/(\Omega A(i)h\nu(i)) \quad (4)$$

where  $A(i)$  is the A-coefficient,  $\nu(i)$  is the frequency of state  $i$ ,  $\Omega$  is the solid angle of the beam, and  $h$  is Planck's constant. Table 2 lists the values for the wavelength ( $\lambda(i)$ ), rotational state ( $J$ ),  $A(i)$ ,  $T_i$ , and  $g(i)$  of the pure rotational levels of H<sub>2</sub> that lie in the wavelength range covered by the IRS low resolution modules.

Figure 2 shows sample excitation diagrams from across the NGC 5194 strip. The excitation diagrams exhibit an ortho-to-para ratio (OPR) of 3 in the nuclear region. This is in agreement with the value of the OPR of the nuclear region determined by SINGS (Roussel et al. 2007, in press). Outside the nucleus, the lower  $J$  (H<sub>2</sub> S(0) - H<sub>2</sub> S(3)) levels exhibit an OPR of 3. The H<sub>2</sub> S(4) measurement shows significant scatter in the excitation diagrams outside of the nuclear region of NGC 5194. This would indicated that the OPR is less than 3; however, due to the low signal-to-noise ratio of the H<sub>2</sub> S(4) map, we do not believe that the OPR determined from the H<sub>2</sub> S(4) intensity reflects the OPR of the warm

$\text{H}_2$ . The excitation-diagrams also exhibit a change in slope as a function of rotational level. This indicates that a continuous distribution of  $\text{H}_2$  temperatures is being sampled within the beam.

Because the excitation diagrams indicate that we are sampling a range of excitation-temperatures in different regions across the NGC 5194 strip, we assume that the  $\text{H}_2$  exists in the form of two discrete components. We define these two components as a warm ( $T = 100 - 300$  K)  $\text{H}_2$  phase and a hot ( $T = 400 - 1000$  K)  $\text{H}_2$  phase. We determine the excitation-temperature and mass distribution of the hot ( $T = 400 - 1000$  K)  $\text{H}_2$  phase from the least squares fit to the  $\text{H}_2 \text{ S}(2) - \text{H}_2 \text{ S}(5)$  lines in the excitation diagram. We determine the excitation-temperature and mass distribution of the warm ( $T = 100 - 300$  K)  $\text{H}_2$  phase from the least squares fit to the  $\text{H}_2 \text{ S}(0) - \text{H}_2 \text{ S}(2)$  lines in the excitation diagram; however, because the warm and hot  $\text{H}_2$  phases are inherently coupled, we subtract the contribution of the hot  $\text{H}_2$  from the warm  $\text{H}_2$  in order to determine the warm  $\text{H}_2$  excitation-temperature and mass (Higdon et al. 2006).

Figure 3 displays the warm (*left*) and hot (*right*)  $\text{H}_2$  mass distributions across the NGC 5194 strip. Mass contours have been overplotted because they are used to compare the locations of the warm and hot  $\text{H}_2$  mass to CO emission (in §4.3), [O IV](25.89  $\mu\text{m}$ ) emission (in §4.4), and X-rays (in §4.5). Note that the non-rectangular shape of the strip is due to the offset between the SL and LL strips. Also, note that the physical stretch of the warm and hot  $\text{H}_2$  mass phases are different. The warm  $\text{H}_2$  mass is determined from the  $\text{H}_2 \text{ S}(0) - \text{H}_2 \text{ S}(2)$  maps which show  $\text{H}_2$  emission across the entire strip. The hot  $\text{H}_2$  mass is determined from the higher  $J$  rotational states from which the  $\text{H}_2$  emission is not well-resolved across the entire strip.

Figure 4 compares the warm  $\text{H}_2$  mass distribution to the excitation-temperature. The gas is warmest in the nuclear region of NGC 5194 with the temperature ranging from 175 -

190 K in the center of the galaxy. The gas is coolest within the spiral arms of NGC 5194. The warm H<sub>2</sub> mass peaks in the inner northwest spiral arm with  $11 \text{ M}_\odot/\text{pc}^2$  warm H<sub>2</sub>. The temperature in this spiral arm decreases from 170 K to 150 K across the arm. We measure significant warm H<sub>2</sub> at large radii from the nucleus of the galaxy. The mass in the outer northwest and southeast spiral arms (at 5 - 6 kpc from the center of the galaxy each) peaks toward the center of the spiral arms with  $3.5 \text{ M}_\odot/\text{pc}^2$  warm H<sub>2</sub> and  $1.0 \text{ M}_\odot/\text{pc}^2$  warm H<sub>2</sub> (in the northwest and southeast arms, respectively) and the gas within the outer spiral arms ranges from 150 K at the center to about 175 K near the edge of the spiral arms.

The excitation-temperature and mass distribution of the hot H<sub>2</sub> reveals a different picture (Figure 5). The peak in hot H<sub>2</sub> mass is bimodal with a peak in the nucleus of the galaxy containing  $0.24 \text{ M}_\odot/\text{pc}^2$  and a second peak that is interior to the inner spiral arm, also containing  $0.24 \text{ M}_\odot/\text{pc}^2$ . The hot H<sub>2</sub> mass in the spiral arms is only a fraction ( $\sim 20$  -  $30 \%$ ) when compared to the mass in the nucleus. The excitation-temperature is 575 K in the nuclear region and the excitation-temperature decreases from the nucleus to the inner spiral arms to  $\sim 500$  -  $550$  K. The hottest excitation-temperatures are observed in the inter-arm regions, where there is the least amount of H<sub>2</sub>.

The ratio of warm-to-hot H<sub>2</sub> mass is not constant across the galaxy. Figure 6 compares the warm H<sub>2</sub> mass distribution (from Figure 3) to the hot H<sub>2</sub> mass distribution (also in Figure 3). The warm mass distribution peaks in the northwest inner spiral arm. The hot mass distribution peaks in the nucleus and in the region interior to the northwest spiral arm. The ratio of warm-to-hot H<sub>2</sub> mass is smallest in the nucleus of the galaxy at 12. Moving from the nucleus to the southeast and northwest spiral arms, the ratio increases to 170 and 136 in the southeast and northwest spiral arms, respectively. The difference in the warm and hot H<sub>2</sub> mass phase distribution and the variations in the morphology of NGC 5194 as a function of rotational energy level ( $J$ ) hint at fundamentally different origins to

the warm and hot H<sub>2</sub> phases. Higher  $J$  lines show stronger intensity in the nuclear region of NGC 5194 where the dominant excitation is likely to be the AGN, shocks associated with the AGN, or high energy photons associated with the AGN. Thus, the warm mass phase and higher  $J$  line emission are more efficiently excited by these more energetic processes. The H<sub>2</sub> S(0) line is much weaker in the nucleus than in the spiral arms. Additionally, the H<sub>2</sub> S(0) and H<sub>2</sub> S(1) lines show strong emission in the spiral arms at large distances from the nucleus of the galaxy. Thus, it is more likely that the warm H<sub>2</sub> mass phase is associated with excitation by photons from star forming regions. The excitation mechanisms are explored in greater detail in §4.3 - §4.5.

To put these results and the maps of the H<sub>2</sub> mass distributions (Figures 3 - 5) in physical context, a typical galactic giant molecular cloud (GMC) contains  $\sim 1 \times 10^6 M_{\odot}$  and is  $\sim 100$  pc in diameter (as observed in the galactic GMC W51 by Carpenter and Sanders (1998)). Such a molecular cloud would have a mass column density of  $30 M_{\odot}/pc^2$ . In the spiral arms of M51, star-formation occurs in giant molecular associations (GMAs). These molecular associations are more massive than typical GMCs and can contain on the order of  $1 \times 10^7 M_{\odot}$  of molecular gas (Rand and Kulkarni 1990). Radii of GMAs can vary from just under 100 pc to several hundred pc and the typical mass column density of a GMA is therefore on the order of  $\sim 300 M_{\odot}/pc^2$ . These mass densities represent the total H<sub>2</sub> mass as determined from CO observations; thus, the mass of the H<sub>2</sub> in the warm and hot phases are only a fraction of the total H<sub>2</sub> in GMAs and GMCs.

The *Spitzer Infrared Nearby Galaxies Survey* (SINGS) has observed H<sub>2</sub> in nearby galaxies (Roussel et al. 2007, in press). Within the central 330 arcsec<sup>2</sup> of NGC 5194, SINGS measures the excitation-temperature and mass of the warm ( $T = 100 - 300$  K) H<sub>2</sub> phase and finds  $T = 180$  K and  $M_{\text{warm}} = 1.46 \times 10^6 M_{\odot}$ . Within the central 412 arcsec<sup>2</sup> of NGC 5194, we measure a warm H<sub>2</sub> excitation-temperature of 186 K and mass of  $1.63 \times 10^6 M_{\odot}$ ,

consistant with the SINGS to within 10 %. SINGS also measures the excitation-temperature of the hot phase (though they do not measure the mass in the hot phase) and find a hot H<sub>2</sub> excitation-temperature of 521 K. Over the nuclear region of NGC 5194, we measure an excitation-temperature of 584 K. Rigopoulou et al. (2002) measures the H<sub>2</sub> mass in the hot phase and find that the warm-to-hot mass fraction varies between  $5 \times 10^3 - 1 \times 10^6$  for Seyferts. This is significantly higher than the warm-to-hot mass fraction (Figure 6) than we measure within the central 412 arcsec<sup>2</sup> of NGC 5194, 14.8. To measure the hot H<sub>2</sub> mass, we use the H<sub>2</sub> S(2) - H<sub>2</sub> S(5) lines, whereas Rigopoulou et al. (2002) uses the H<sub>2</sub> S(5) - H<sub>2</sub> S(7) lines. Thus, the hot H<sub>2</sub> phase that they measure is preferentially offset to higher H<sub>2</sub> excitation-temperatures and lower H<sub>2</sub> masses. We would like to note that in NGC 5194, within a 10''.2 beam, we are sensitive to  $0.40 M_{\odot}/pc^2$  warm H<sub>2</sub> and  $0.005 M_{\odot}/pc^2$  hot H<sub>2</sub> (though the sensitivity to the hot H<sub>2</sub> could be underestimated due to smoothing the H<sub>2</sub> S(2), H<sub>2</sub> S(3), H<sub>2</sub> S(4), and H<sub>2</sub> S(5) lines by a factor of 2 - 4 times their resolution).

#### 4.2. Distinguishing the H<sub>2</sub> Excitation Mechanisms

Previous studies of pure rotational H<sub>2</sub> emission in galaxies have used aperture average spectra over the central regions of galaxies to understand the distribution of the warm and hot molecular gas phases within a galaxy (Rigopoulou et al. 2002, Higdon et al. 2006, Roussel et al. 2007, in press). These studies use the pure rotational lines to derive excitation-temperatures and warm and hot H<sub>2</sub> masses within the galaxy. Additionally, these studies compare the warm and hot H<sub>2</sub> mass to the cold H<sub>2</sub> mass traced by CO emission in order to understand the mass fractions of the cold ( $T = 5 - 10$  K), warm, and hot H<sub>2</sub> mass. While these studies have yeilded tremendous insight into the mass fractions of the different temperature phases of H<sub>2</sub> in galaxies, they have had difficulty distinguishing the H<sub>2</sub> excitation mechanisms within the galaxies.

$\text{H}_2$  is generally excited via four processes: 1.) excitation in photodissociation regions (PDRs) , 2.) shocks, 3.) X-ray dissociation (XDRs), and 4.) cosmic rays. Mapping the warm and hot  $\text{H}_2$  excitation-temperature and mass distributions provides the information necessary to understand whether the warm and hot  $\text{H}_2$  phases undergo excitation via the same mechanism. This information coupled with spatially resolved diagnostics of PDRs, shocks, and XDRs place constraints on the dominant  $\text{H}_2$  excitation mechanism in NGC 5194, in different regions within NGC 5194.

Variations in the morphology of the  $\text{H}_2$  line emission and the differences between the warm and hot  $\text{H}_2$  excitation temperature and mass distributions indicate that the primary excitation mechanisms of the different  $\text{H}_2$  phases vary across a galaxy. In order to understand the excitation mechanisms of the warm  $\text{H}_2$  and the hot  $\text{H}_2$  phases and where each is dominant, we present comparisons of the  $\text{H}_2$  line intensity and mass distributions to diagnostics of three excitation mechanisms (PDRs, shocks, and XDRs). CO rotational transitions are used as diagnostic lines of PDRs (Allen et al. 2004). Comparing the  $\text{H}_2$  mass distributions to CO ( $J = 1 - 0$ ) thus compares the location of the  $\text{H}_2$  mass to locations of GMAs and GMCs. The [O IV](25.98  $\mu\text{m}$ ) line can be excited in shocks (Schaerer and Stasinska 1999). Spatial mapping of [O IV](25.89  $\mu\text{m}$ ) emission thus serves to discern regions where  $\text{H}_2$  is excited primarily by shocks.  $\text{H}_2$  excitation by X-rays can also be discerned within NGC 5194 by comparing the  $\text{H}_2$  mass phases and emission to X-ray emission observed by the Chandra X-ray Observatory (Terashima and Wilson 2001). The following sections compare the  $\text{H}_2$  mass distributions to CO ( $J = 1 - 0$ ) emission, [O IV](25.89  $\mu\text{m}$ ) emission, and X-ray emission.

### 4.3. H<sub>2</sub> Excitation by PDRs: Comparison of H<sub>2</sub> to CO emission

Within a molecular cloud, H<sub>2</sub> exists within the PDR and deep into the molecular cloud. Owing to an ionization potential of 4.5 eV, H<sub>2</sub> formation generally does not occur within a PDR until the radiation field becomes sufficiently weak. The H<sub>2</sub> - PDR connection has become the emphasis of many theoretical models. Recent advances in the CLOUDY photoionization modeling code have included H<sub>2</sub> and modeled the structure of star forming regions while treating the HII region and PDR as one continuous cloud (Shaw et al. 2005, Abel et al. 2005). Kaufman et al. (2006) used Starburst99/Mappings to model H<sub>2</sub> pure rotational line emission from PDRs to probe the conditions of dense PDRs in star forming regions. They show that within galaxies, where the telescope beam size is generally kiloparsecs across, H<sub>2</sub> emission could serve to probe the surface layers of dense molecular clouds.

CO emission arises from deep within a molecular cloud where the temperatures are too cold to excite H<sub>2</sub> emission. In these regions, CO is collisionally excited by the much more abundant H<sub>2</sub> molecule. Thus, molecular gas within molecular clouds has generally been studied via observations of CO rotational line emission. Here, we compare the warm and hot H<sub>2</sub> mass phases and H<sub>2</sub> rotational line emission to CO ( $J = 1 - 0$ ) emission (mapped by BIMA SONG) in order to understand the relationship between H<sub>2</sub> emission and PDRs.

Figure 7 compares the warm (*left*) and hot H<sub>2</sub> (*right*) mass distributions to CO emission. Within the spiral arms, the H<sub>2</sub> mass is generally aligned with CO emission; however, there are offsets in the location of the peaks in the H<sub>2</sub> mass and CO emission. This is real and is not due to the difference in resolution between the CO map (6'') and the H<sub>2</sub> maps (10''.2). In the northwest inner spiral arm, the peak in warm H<sub>2</sub> mass is offset to the northwest of the peak in CO emission. At even larger distances from the nucleus of NGC 5194, we observe the H<sub>2</sub> mass offset from the CO emission within the outer northwest spiral

arm. In this case, the  $H_2$  mass is offset to the southeast of the CO emission. Additionally, in the southeast outer spiral arm we observe  $H_2$  in a region that appears devoid of CO emission. These regions, where the peaks are offset or there is no CO emission where  $H_2$  is observed could just be spiral arms that are rich in  $H_2$  but devoid of CO. Comparing the hot  $H_2$  mass phase to CO emission (Figure 7, *right*), the hot  $H_2$  mass peaks in the nucleus and in the region interior to the CO spiral arm. In the northwest and southeast spiral arms, CO emission is found within the wider  $H_2$  mass contours. This is a result of the difference in resolution between the  $H_2$  maps and the BIMA SONG CO map.

Figure 8 compares the CO intensity to the  $H_2$  S(0) -  $H_2$  S(3) rotational line intensity. These maps all resolve  $H_2$  emission within the nucleus and spiral arms of the galaxy. The  $H_2$  S(2) and  $H_2$  S(3) maps (at resolutions of  $3.^{\prime\prime}44$  and  $4.^{\prime\prime}37$ , respectively) show strong correlation between  $H_2$  and CO emission within the spiral arms. In the spiral arms, the  $H_2$  emission generally traces the CO emission with the one exception that in the  $H_2$  S(2) map,  $H_2$  emission in the southeast spiral arm is offset to the southeast by  $2.^{\prime\prime}$  from the CO spiral arm. Comparing the  $H_2$  S(1) map to CO emission shows that a strong correlation between  $H_2$  and CO emission in the spiral arms. In this case both maps are at similar resolutions ( $\sim 6.^{\prime\prime}$ ) and the  $H_2$  contours trace the CO emission (though it should be noted that the  $H_2$  contours appear wider than the CO emission; this is an effect of grouping spectra prior to fitting). The comparison between the  $H_2$  S(0) and CO emission shows that the  $H_2$  S(0) and CO emission are correlated; however, we notice offsets in the emission peaks for CO and  $H_2$  S(0). While we notice offsets between the  $H_2$  S(0) and CO emission peaks, a correlation between  $H_2$  and CO emission in the spiral arms is evident. In general, the  $H_2$  emission traces the CO spiral arms and except for in the southwest spiral arm, the  $H_2$  S(2) and  $H_2$  S(3) emission from the spiral arms is co-spatial with the CO emission. This suggests that the  $H_2$  emission in the spiral arms is associated with the surface layers of PDRs, as predicted by Kaufman et al. (2006).

While H<sub>2</sub> rotational line emission and CO are correlated in the spiral arms, the peaks in H<sub>2</sub> S(2) and H<sub>2</sub> S(3) intensity both occur in the nucleus of NGC 5194. Within the H<sub>2</sub> S(2) and H<sub>2</sub> S(3) emission peaks, faint CO emission is offset to the north of the H<sub>2</sub> intensity peaks. This suggests that while H<sub>2</sub> emission is excited within PDRs associated with dense molecular clouds in the spiral arms, a different process is the dominant excitation mechanism of the higher  $J$  lines and the hot H<sub>2</sub> phase within the nuclear region of NGC 5194.

#### 4.4. H<sub>2</sub> Excitation by Shocks: Comparison of H<sub>2</sub> to [OIV](25.89 $\mu\text{m}$ ) emission

The [O IV](25.89  $\mu\text{m}$ ) line can be excited in shocks, the stellar winds of massive Wolf-Rayet stars, or by an active galactic nucleus (AGN)(Schaerer and Stasinska 1999, Lutz et al. 1998, Smtih et al. 2004). Though the [O IV](25.89  $\mu\text{m}$ ) line is bledened with the [Fe II](25.99  $\mu\text{m}$ ) line in *Spitzer* IRS low resolution spectra, PAHFIT can deblend the two lines. Thus, in mapping the H<sub>2</sub> S(0) and H<sub>2</sub> S(1) line in the LL data cubes, [O IV](25.89  $\mu\text{m}$ ) emission was also be mapped at a resolution of 9''.39 ( $\lambda/\delta\lambda = 142$ ).

Figure 9 compares [O IV](25.89  $\mu\text{m}$ ) intensity to the warm and hot H<sub>2</sub> disributions. The [O IV](25.89  $\mu\text{m}$ ) line intensity map, warm H<sub>2</sub> map, and hot H<sub>2</sub> map all have comparable resolutions (9''.39, 10''.2, and 10''.2, respectively). The [O IV](25.89  $\mu\text{m}$ ) emission is brightest in the central region of the galaxy and its peak is co-spatial with the nuclear peak in the mass of the hot H<sub>2</sub>. Moving from the nucleus to the inner spiral arm, the [O IV](25.89  $\mu\text{m}$ ) emission subsides. Note also weak [O IV](25.89  $\mu\text{m}$ ) emission within the hot H<sub>2</sub> spiral arms and in the inter-arm region (toward the southeast spiral arm).

[O IV](25.89  $\mu\text{m}$ ) emission within the nuclear region is likely due to the weak Seyfert 2 nucleus (Ford et al. 1985) and is possibly associated with shocked gas from the outflows

of the AGN. The peak of the [O IV](25.89  $\mu\text{m}$ ) emission coincides with the nuclear peak in hot H<sub>2</sub> mass indicating that the hot H<sub>2</sub> phase in the nuclear region of the galaxy is AGN or shock heated. With about  $2.43 \times 10^5 M_{\odot}$  of hot H<sub>2</sub> in the central 0.58 kpc<sup>2</sup>, it is unlikely that the hot H<sub>2</sub> is fueling the central AGN, but rather is excited by the AGN or shocks produced by it. In the nuclear region we observe a factor of 15 times greater warm H<sub>2</sub> mass. While there is significantly more mass in the warm phase, the warm H<sub>2</sub> mass is much greater within the spiral arms than within the nucleus. Thus, in the nuclear region, shocks appear to be a less efficient means to excite the warm phase than the hot phase.

#### 4.5. H<sub>2</sub> Excitation by XDRs: Comparison of H<sub>2</sub> to X-ray emission

M51 has been extensively studied in X-rays by ASCA (Terashima et al. 1998), Newton XMM (Dewangen et al. 2005), and the Chandra X-ray Observatory (Terashima and Wilson 2001). These observations of the M51a,b system have revealed more than 80 X-ray sources. Candidates for these X-ray sources include neutron stars, black holes, supernova remnants (SN 1994I), and a low-luminosity AGN (Terashima et al. 2006, Immler et al. 2002, Terashima and Wilson 2001). X-ray emission from the nuclear region of NGC 5194 has been studied by Terashima and Wilson (2001). At  $\sim 1''$  resolution, they observe X-ray emission from the nucleus, the extranuclear cloud (XNC, to the south of the nucleus), and the northern loop. A radio jet has been observed connecting the nucleus of NGC 5194 to the XNC in 6 cm imagery (Crane and van der Hulst 1992). The jet emanates from the south of the elongated nucleus and is shock heating ISM.

Figure 10 compares the smoothed 0.5 - 10 keV x-ray band image to the warm (*left*) and hot (*right*) H<sub>2</sub> mass distributions. The 0.5 - 10 keV band has been smoothed to the resolution of the warm and hot H<sub>2</sub> mass distributions. Consequently, the nucleus, XNC, and northern loop are indistinguishable in the smoothed image. There is very little correlation

between the 0.5 - 10 keV X-ray band and the warm H<sub>2</sub> mass distribution. X-ray emission is most intense from the nucleus and decreases into the northwest spiral arm that contains the greatest H<sub>2</sub> mass. X-ray emission does correlate with the hot H<sub>2</sub> mass. The most intense 0.5 - 10 keV X-ray emission originates from the nucleus and is oriented north-to-south, similar to the [O IV](25.89  $\mu$ m) emission. The peak in X-ray emission is located within the peak in hot H<sub>2</sub> mass. The correlation between X-ray emission from the nucleus of NGC 5194 and the peak in hot H<sub>2</sub> mass suggests that X-rays play an important role in exciting the hot phase of H<sub>2</sub>. However, while there is a correlation between X-ray emission and the hot H<sub>2</sub> phase, H<sub>2</sub> excitation by X-rays cannot be distinguished from H<sub>2</sub> excitation by shocks. When smoothed to 10''.2 resolution, the X-ray distribution mimics the [O IV](25.89  $\mu$ m) emission map.

In order to further investigate X-ray excited H<sub>2</sub> emission in the nuclear region of NGC 5194, we compare the X-ray image (at 1'' resolution) to the H<sub>2</sub> S(2) - H<sub>2</sub> S(5) intensity maps (Figure 11). The H<sub>2</sub> S(2), H<sub>2</sub> S(3), H<sub>2</sub> S(4), and H<sub>2</sub> S(5) line intensities all peak at the X-ray source within the nucleus. The X-ray source fits within the H<sub>2</sub> contours because the X-ray image resolution is higher than the resolution of each of the H<sub>2</sub> maps. The morphology of the nuclear H<sub>2</sub> emission is correlated with the X-ray source. The H<sub>2</sub> S(2) intensity peaks around the X-ray nucleus. The intensity decreases to the south and falls off by 70 % within the southern XNC. The bar structure seen in the H<sub>2</sub> S(3) emission correlates with X-ray emission. The H<sub>2</sub> S(3) intensity peaks between the X-ray nucleus and the XNC. To the north of the nucleus, the contours follow the X-ray loop. Additionally, H<sub>2</sub> S(3) intensity decreases by 80 % from the nucleus to the south of the XNC. Both the H<sub>2</sub> S(4) and H<sub>2</sub> S(5) maps show that the peak in intensity are co-spatial with the peaks in X-ray emission.

## 5. Conclusions

We have spectrally mapped a strip across NGC 5194 using the *Spitzer* IRS low resolution modules. We used the spatially resolved spectra to map H<sub>2</sub> S(0) - H<sub>2</sub> S(5) line intensities across the strip. We find:

1. The morphology of H<sub>2</sub> emission in NGC 5194 varies with H<sub>2</sub> rotational level. H<sub>2</sub> S(0) emission is strongest in the spiral arms of the galaxy while the higher  $J$  transitions show the strongest emission towards the nucleus. The H<sub>2</sub> S(0) and H<sub>2</sub> S(1) maps (at 10''.2 and 6''.17 resolution, respectively) show emission across the entire strip out to spiral arms located 5 - 6 kpc from the center of the galaxy. The H<sub>2</sub> S(2) and H<sub>2</sub> S(3) maps (at 4''.37 and 3''.44 resolution, respectively) reveal H<sub>2</sub> emission in the nucleus, spiral arms, and inter-arm regions of NGC 5194. Strong H<sub>2</sub> S(4) and H<sub>2</sub> S(5) emission is resolved in the nuclear region of NGC 5194. The H<sub>2</sub> maps reveal interesting morphology to the molecular gas distributions, such as bar structure across the nucleus in H<sub>2</sub> S(3) emission.
2. The different morphologies of H<sub>2</sub> emission in NGC 5194 indicate variations in H<sub>2</sub> excitation-temperature and mass. Excitation diagrams reveal that the H<sub>2</sub> exists in a continuous distribution of temperatures across the galaxy. We assume that the H<sub>2</sub> exists in the form of two phases, a warm ( $T = 100 - 300$  K) phase and a hot ( $T = 400 - 1000$  K) phase. Mapping the excitation-temperature and mass distributions of both the warm and hot H<sub>2</sub> phases across the NGC 5194 strip reveals the greatest amount of warm H<sub>2</sub> in the northwest inner spiral arm ( $11 M_{\odot}/pc^2$ ) and the greatest amount of hot H<sub>2</sub> in the nuclear region and the region interior to the northwest inner spiral arm ( $0.24 M_{\odot}/pc^2$ ). The mass column densities of the warm and hot H<sub>2</sub> are only a fraction of the total molecular gas mass content of GMAs in M51. The excitation-temperature of the warm and hot phases vary across the galaxy with the warm phase

peaking in the nucleus at 192 K and the hot phase peaking in the inter-arm regions at 960 K.

3. The warm and the hot H<sub>2</sub> mass are not co-spatial. The hot mass distribution shows two peaks, one in the nucleus of NGC 5194 and one located interior to the northwest inner spiral arm of NGC 5194. The warm mass distribution peaks in the northwest spiral arm. The warm-to-hot mass ratio varies across the galaxy with the ratio being  $\sim 15$  in the nucleus and increasing to  $\sim 100$  in the spiral arms. Variations in the warm-to-hot H<sub>2</sub> ratio and differences in the morphology of the H<sub>2</sub> emission across NGC 5194 indicate that the primary excitation mechanism differs for the warm and hot H<sub>2</sub> mass phases as a function of location within the galaxy.
4. The warm H<sub>2</sub> mass phase correlates with the CO emission within the spiral arms. Within the spiral arms, the H<sub>2</sub> is associated with the CO emission indicating that the H<sub>2</sub> emission is most likely associated with the surface layers of dense PDRs. However, there are offsets in the location of the peaks in H<sub>2</sub> mass and CO emission. These offsets are real and are possibly associated with regions that are rich in H<sub>2</sub> but devoid of CO.
5. [O IV](25.89  $\mu$ m) emission and X-ray emission both correlate with the hot H<sub>2</sub> mass suggesting that the hot H<sub>2</sub> in the nucleus is primarily excited by the AGN, strong shocks (possibly associated with the central AGN), or X-rays associated with the AGN. The [O IV](25.89  $\mu$ m) emission and X-ray image are very similar and thus a primary excitation mechanism (shocks or XDRs) of the hot H<sub>2</sub> mass phase cannot be distinguished. Further comparison of the H<sub>2</sub> S(2) - H<sub>2</sub> S(5) intensity maps to X-ray emission reveal that the nuclear H<sub>2</sub> emission is associated with the X-ray emission from the nucleus of NGC 5194.

The author graciously acknowledges the Spitzer Science Center Spitzer Visiting Graduate Student Fellowship Program and committee for providing support for this research. The author would like to specifically acknowledge the program coordinators, Phil Appleton and Alberto Noriega-Crepso. The author would also like to thank JD Smith for swift responses to questions about PAHFIT and CUBISM and Nicolas Flagey for productive discussions about PAHFIT.

*Facilities:* Spitzer Science Center (SSC), Spitzer Space Telescope (SST), Berkely-Illinois-Maryland Array (BIMA).

## REFERENCES

- Aalto, S., Hüttemeister, S., Scoville, N.Z., and Thaddeus, P., 1999, AJ, 522, 165
- Abel, N.P., Ferland, G.J., Shaw, G., and van Hoof, P.A.M., 2005, ApJS, 161, 65
- Allen, R.J., Heaton, H.I., and Kaufman M.J., 2004, ApJ, 608, 314
- Blitz, L., 1995, SSR, 684
- Calzetti, D. et al., 2005, ApJ, 633, 871
- Carpenter, J.M. and Sanders, D.B., 1998, AJ, 116, 1856
- Crane, P.C. and van der Hulst, J.M., 1992, AJ, 103, 1146
- Davies, R.I., Sternberg, A., Lehnert, M., and Tacconi-Garman, L.E., 2003, ApJ, 597, 907
- Dewangan, G.C., Griffiths, R.E., Choudhury, M., Miyaji, T., and Schurch, N.J., 2005, ApJ, 635, 198
- Ford, H.C., Crane, P.C., Jacoby, G.H., Lawrie, D.G., and van der Hulst, J.M., 1985, ApJ, 293, 132
- Fuente et al., 1999, ApJ, 518, L45
- Helfer, T.T. and Blitz, L., 1997,
- Helfer, T.T., Thornley, M.D., Regan, M.W., Wong, T., Sheth, K., Vogel, S.N., Blitz, L., and Bock, D.C.J., 2003, ApJS, 145, 259
- Higdon, S.J.U., Armus, L., Higdon, J.L., Soifer, B.T., and Spoon, H.W.W., 2006, ApJ, 648, 323
- Houck, J.R. et al., 2004, ApJS, 145, 18

- Immler, S., Wilson, A.S., and Terashima, Y., 2002, ApJ, 573, L27
- Kaufman, M.J., Wolfire, M.G., and Hollenbach, D.J., 2006, ApJ, 644, 283
- Lord, S.D. and Young, J.S., 1990, ApJ, 356, 135
- Lutz, D., Kunze, D., Spoon, H.W.W., and Thornley, M.D., 1998, A&A, 333, L75
- Kennicutt, R.C. et al., 2003, PASP, 115, 928
- Kenny, J.D.P. and Lord, S.D., 1991, ApJ, 381, 118
- Matsushita, S. et al., 2004, ApJ, 616, L55
- Moorwood, A.F.M. and Oliva, E., 1990, A&A, 239, 78
- Murphy, E.J. et al., 2006, ApJ, 638, 157
- Neufeld, D.A., Melnich, G.J., Sonnentrucker, P., Bergin, E.A., Green, J.D., Kim, K.H., Watson, D.M., Forrest, W.J., and Pipher, J.L., 2006, ApJ, 649, 816
- Pak, S., Jaffe, D.T., Stacey, G.J., Bradford, C.M., Klumpe, E.W., and Keller, L.D. 2004, ApJ, 609, 692
- Palumbo, G.G.C., Fabbiano, G., Fransson, C., and Trinchieri, G., 1985, ApJ, 298, 259
- Rand, R.J. and Kulkarni, S.R., 1990, ApJ, 349, L43
- Regan, M.W., Thornley, M.D., Helfer, T.T., Sheth, K., Wong, T., Vogel, S.N., Blitz, L., and Bock, D.C.J., 2001, ApJ, 561, 218
- Rigopoulou, D., Kunze, D., Lutz, D., Genzel, R., and Moorwood, A.F.M., 2002, A&A, 389, 374
- Roussel, H. et al., 2007, in press

Schaerer, D. and Stasinska, G., 1999, A&A, 345, L17

Scoville, N.Z. and Young, J.S., 1983, AJ, 265, 148

Scoville, N.Z., Yun, M.S., Armus, L., and Ford, H., 1998, ApJ, 493, L63

Scoville, N.Z., Polletta, M., Ewald, S., Stolovy, S.R., Thompson, R., and Rieke, M., 2001,  
AJ, 122, 3017

Shaw, G., Ferland, G.J., Abel, N.P., Stancil, P.C., and van Hoof, P.A.M., 2005, ApJ, 624,  
794

Sheth, K., Regan, M.W., Vogel, S.N., and Teuben, P.J., 2000, ApJ, 532, 221

Sheth, K., Vogel, S.N., Regan, M.W., Thornley, M.D., and Teuben, P.J., 2005, ApJ, 632,  
217

Smith, J.D.T. et al., 2004, ApJS, 154, 199

Smith, J.D.T., Armus, L., Buckalew, B., Dale, D.A., Helou, G., Roussel, H., and Sheth, K.,  
2006, CUBISM User Manual

Smith, J.D.T. et al., 2007, ApJ, 656, 770

Smith, J.D.T. et al., 2007, in press

Sternberg, A. and Neufeld, D.A., 1999, ApJ, 516, 371

Terashima, Y., Ptak, A., Fujimoto, M.I., Kunieda, H., Makishima, K., and Sherlemitsos,  
P.J., 1998, ApJ, 496, 210

Terashima, Y. and Wilson, A.S., 2001, ApJ, 560, 139

Vogel, S.N., Kulkarni, S.R., and Scoville, S.Z., 1988, Nature, 334, 402

Terashima, Y. and Wilson, A.S., 2001, ApJ, 560, 139

Young, J.S. and Devereux, N.A., 1991, ApJ, 373, 414

Young, J.S. and Scoville, N.Z., 1991, ARA&A, 29, 581

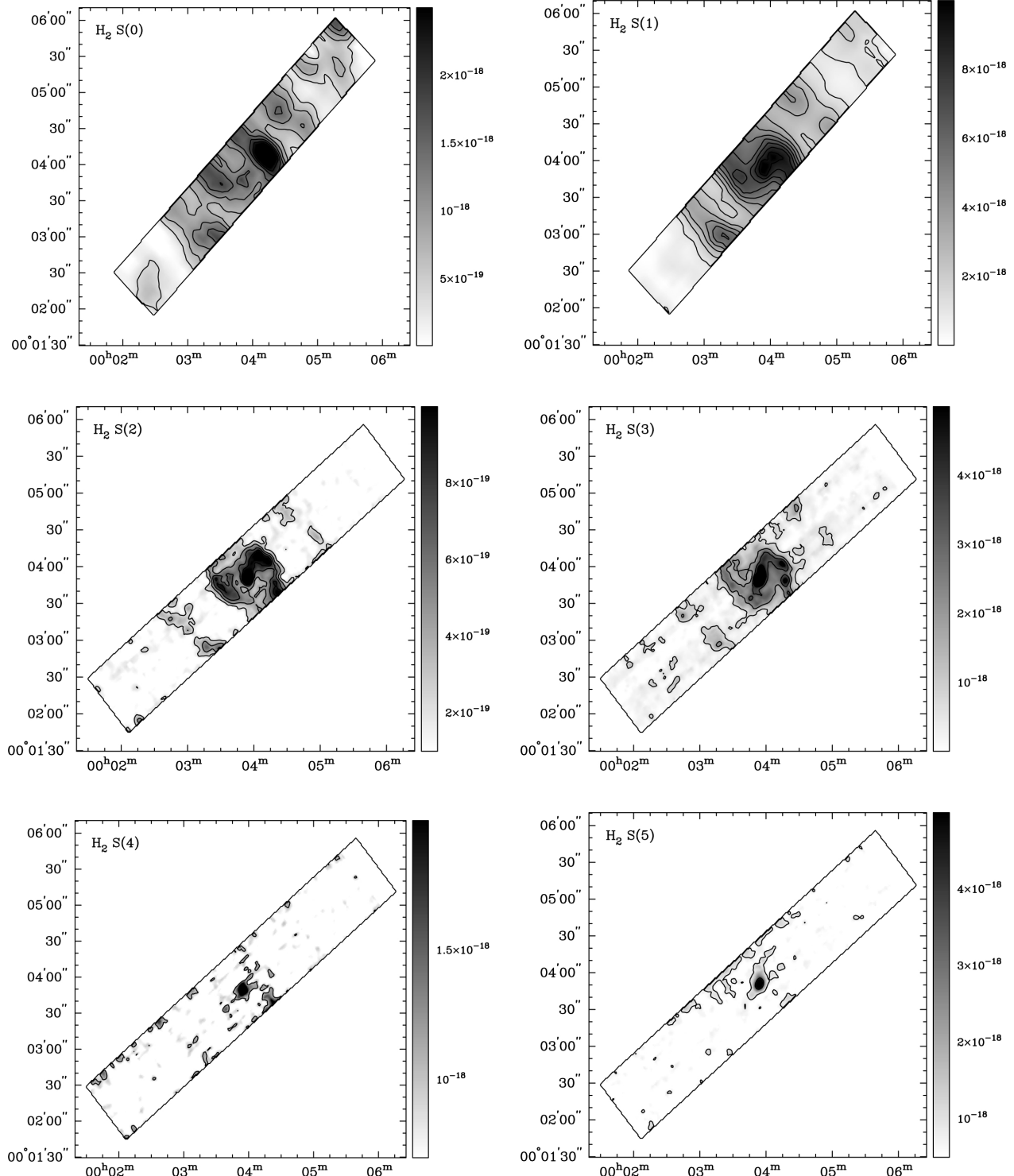


Fig. 1.— Maps of the H<sub>2</sub> S(0) (*top left*), H<sub>2</sub> S(1) (*top right*), H<sub>2</sub> S(2) (*middle left*), H<sub>2</sub> S(3) (*middle right*), H<sub>2</sub> S(4) (*bottom left*), and H<sub>2</sub> S(5) (*bottom right*) intensity across the SL and LL strips that were mapped with the Spitzer IRS. The H<sub>2</sub> S(0) and H<sub>2</sub> S(1) maps are created from the LL data cubes. The resolution of the H<sub>2</sub> S(0) and H<sub>2</sub> S(1) maps are 10''.2 and 6''.17, respectively. The H<sub>2</sub> S(2), H<sub>2</sub> S(3), H<sub>2</sub> S(4), and H<sub>2</sub> S(5) maps are created from the SL data cube. The resolution of the H<sub>2</sub> S(2), H<sub>2</sub> S(3), H<sub>2</sub> S(4), and H<sub>2</sub> S(5) maps are 4''.37, 3''.44, 2''.85, and 2''.46, respectively. The grey-scale is in units of W/m<sup>2</sup>. Contour levels are at  $2.9 \times 10^{-18}$ ,  $2.2 \times 10^{-18}$ ,  $1.8 \times 10^{-18}$ ,  $1.5 \times 10^{-18}$ ,  $1.1 \times 10^{-18}$ ,  $7.3 \times 10^{-19}$ , and  $3.7 \times 10^{-19}$  W/m<sup>2</sup> for H<sub>2</sub> S(0);  $9.6 \times 10^{-18}$ ,  $8.6 \times 10^{-18}$ ,  $7.5 \times 10^{-18}$ ,  $6.4 \times 10^{-18}$ ,  $5.4 \times 10^{-18}$ ,  $4.3 \times 10^{-18}$ ,  $3.2 \times 10^{-18}$ ,  $2.1 \times 10^{-18}$  and  $1.1 \times 10^{-18}$  W/m<sup>2</sup> for H<sub>2</sub> S(1);  $1.1 \times 10^{-18}$ ,  $8.9 \times 10^{-19}$ ,  $6.7 \times 10^{-19}$ ,  $4.4 \times 10^{-19}$ , and  $2.2 \times 10^{-19}$  W/m<sup>2</sup> for H<sub>2</sub> S(2);  $1.21 \times 10^{-17}$ ,  $9.4 \times 10^{-18}$ ,  $6.7 \times 10^{-18}$ ,  $4.0 \times 10^{-18}$ , and  $1.3 \times 10^{-18}$  W/m<sup>2</sup> for H<sub>2</sub> S(3);  $2.0 \times 10^{-18}$  and  $1.0 \times 10^{-18}$  W/m<sup>2</sup> for H<sub>2</sub> S(4);  $7.3 \times 10^{-18}$ ,  $4.0 \times 10^{-18}$ , and  $8.0 \times 10^{-19}$  W/m<sup>2</sup> for H<sub>2</sub> S(5). The vertical axis is the right ascension and the horizontal axis is the declination. Note that in all of the maps, north is up and west is to the left. The box around the intensity maps represents the SL or LL strip that was mapped.

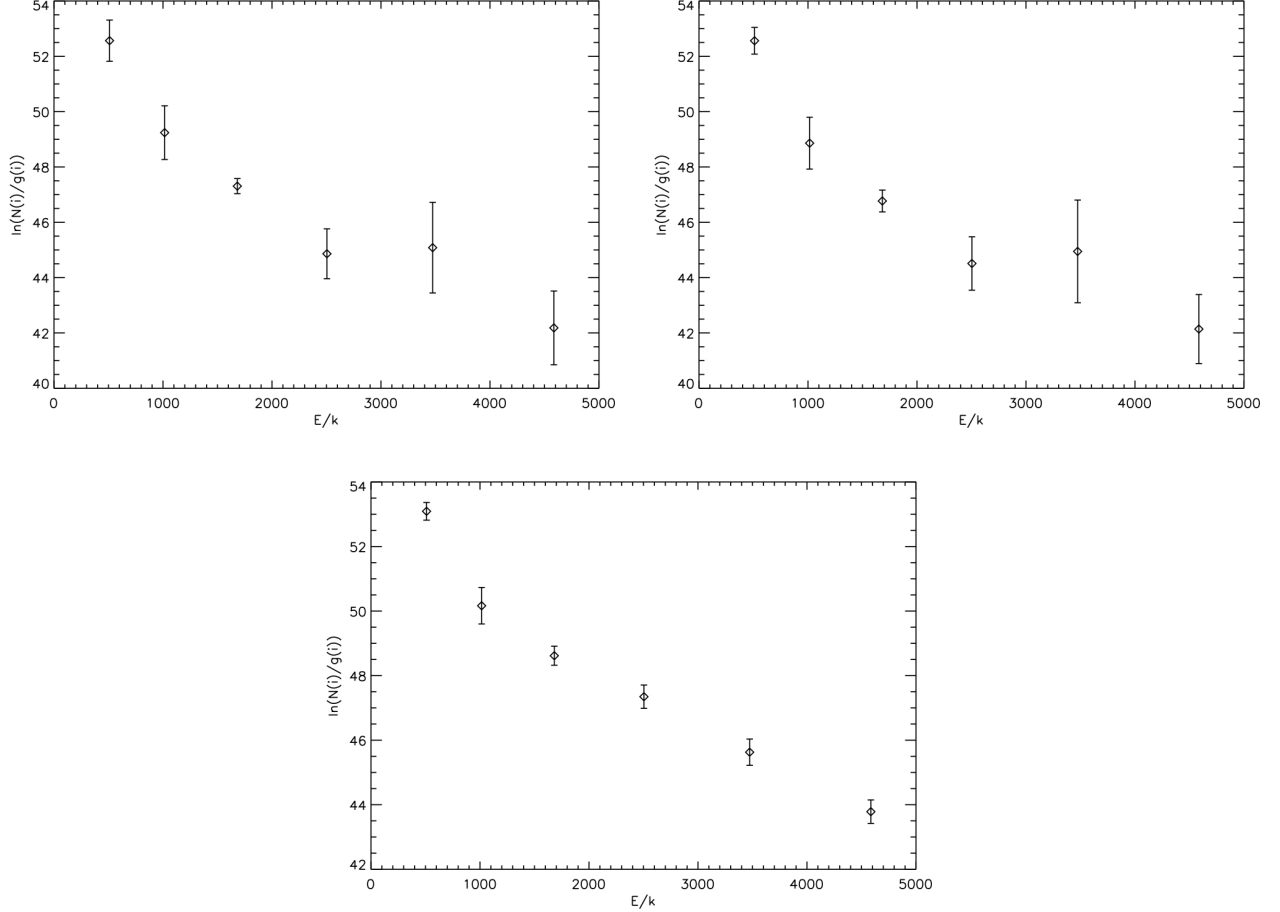


Fig. 2.— Sample excitation diagrams taken from different regions along the NGC 5194 strip. The top two excitation diagrams are taken from regions within the southeast and northwest spiral arms that are  $10''.2$  in diameter ( $1.13 \times 10^5$  pc $^2$ ) and centered at (RA, Dec) of (202.45, 47.21) and (202.49, 47.18), respectively. The excitation diagram at the bottom is taken from the nuclear region. The aperture is  $10''.2$  in diameter ( $1.13 \times 10^5$  pc $^2$ ), centered at (RA, Dec) of (202.47, 47.19).

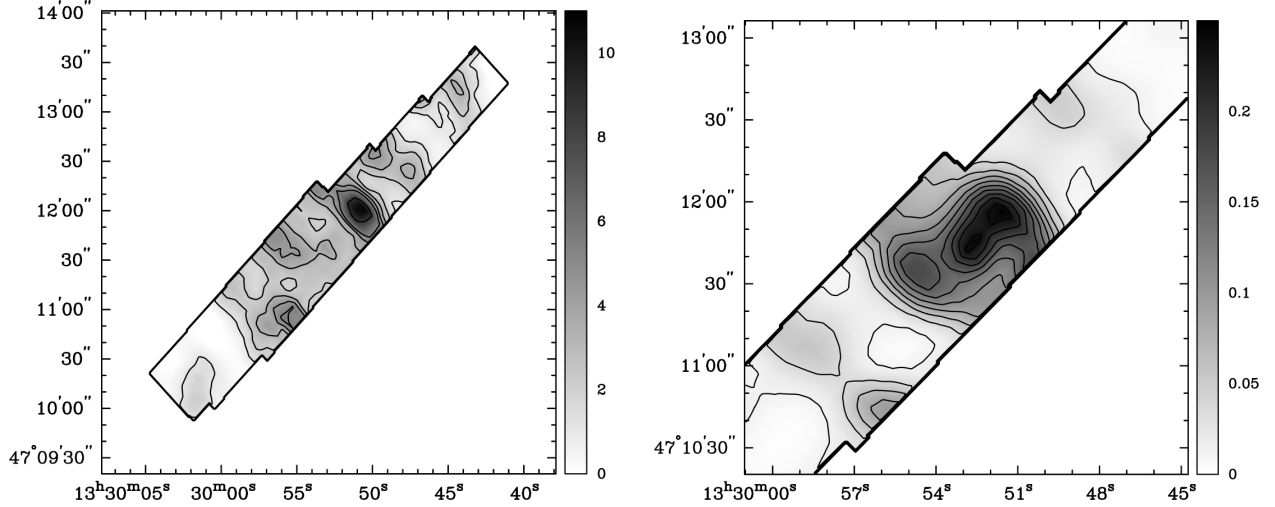


Fig. 3.— Shown are the warm ( $T = 100 - 300 \text{ K}$ )  $\text{H}_2$  (*left*) and hot ( $T = 400 - 1000 \text{ K}$ )  $\text{H}_2$  (*right*) mass distributions. The mass distributions are in units of  $M_{\odot}/\text{pc}^2$ . Contours are overplotted for clarity. The warm  $\text{H}_2$  mass contour levels are at 8.85, 5.55, 4.43, 3.32, 2.21, and  $1.10 M_{\odot}/\text{pc}^2$ . The hot  $\text{H}_2$  contour levels are at 10 % of  $0.25 M_{\odot}/\text{pc}^2$ . The hot  $\text{H}_2$  mass distribution is derived from the fit to the  $\text{H}_2 \text{ S}(2) - \text{H}_2 \text{ S}(5)$  lines and the warm  $\text{H}_2$  mass distribution is derived from the fit to the  $\text{H}_2 \text{ S}(0) - \text{H}_2 \text{ S}(2)$  lines, corrected for the contribution of the hot  $\text{H}_2$  mass phase.

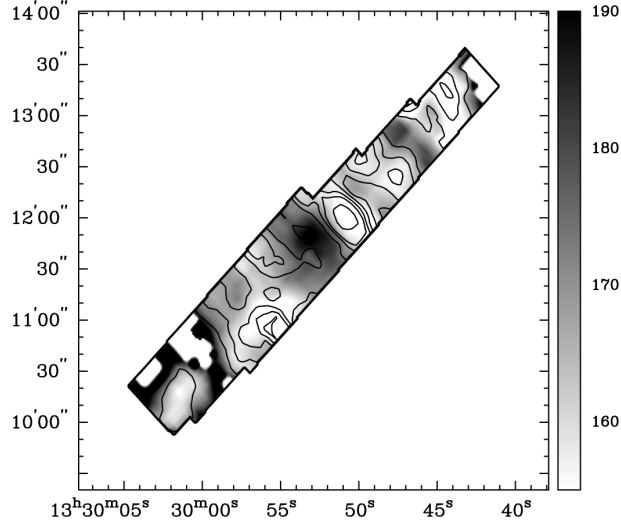


Fig. 4.— The warm ( $T = 100 - 300$  K)  $H_2$  mass distribution compared to the warm  $H_2$  excitation-temperature. The warm  $H_2$  excitation-temperature and mass distributions are derived from the fit to the excitation diagrams across the strip for the  $H_2$  S(0) -  $H_2$  S(2) lines, corrected for the contribution of the hot ( $T = 400 - 1000$  K)  $H_2$  phase. Mass density contour levels are at 8.85, 5.55, 4.43, 3.32, 2.21, and  $1.10 M_\odot/\text{pc}^2$  (same as in Figure 3). The grey-scale represents the excitation-temperature distribution (in units of Kelvin). The non-rectangular shape to the map is due to the slight offset of the *Spitzer* IRS SL strip relative to the LL strip.

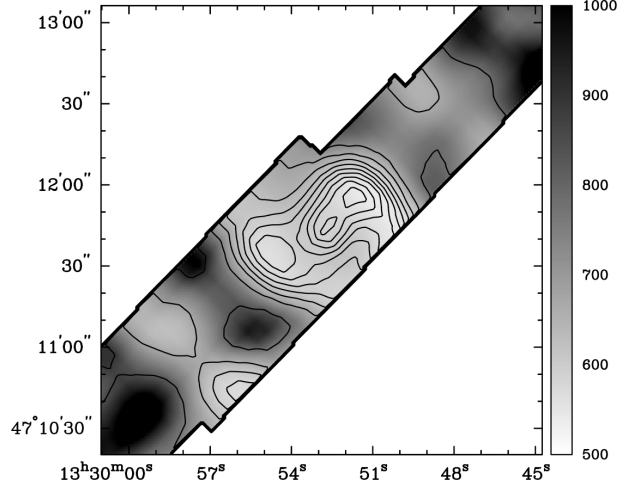


Fig. 5.— The hot ( $T = 400 - 1000$  K)  $H_2$  mass distribution compared to the hot  $H_2$  excitation-temperature. The hot  $H_2$  excitation-temperature and mass distributions are derived from the fit to the excitation diagrams across the strip for the  $H_2$  S(2) -  $H_2$  S(5) lines. Mass density contour levels are at 10% of  $0.25 M_\odot/\text{pc}^2$  (same as in Figure 3). The grey-scale represents the excitation-temperature distribution (in units of Kelvin). Note that the due to lack of  $H_2$  detection from the higher  $J$  lines at greater distances from the nucleus of NGC 5194, we are unable to map the hot  $H_2$  distributions across the entire strip as we have done for the warm  $H_2$  distribution.

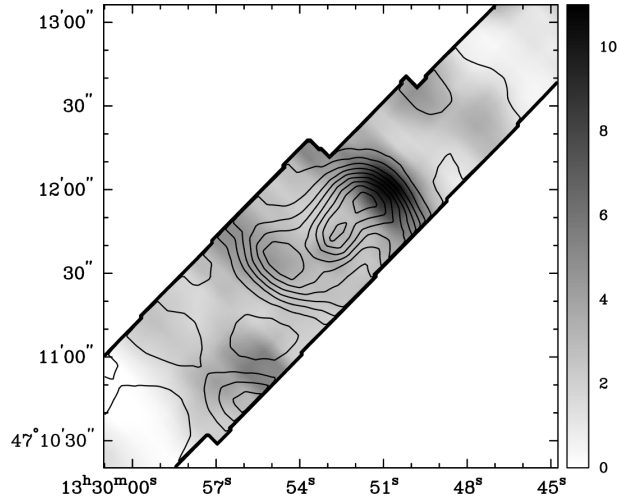


Fig. 6.— The warm ( $T = 100 - 300$  K)  $H_2$  mass (in grey-scale, same as in Figure 3) compared to the hot ( $T = 400 - 1000$  K)  $H_2$  mass (in contours, same is in Figure 3). Contours levels for the hot  $H_2$  mass distribution are at 10% of the maximum mass density  $0.25 M_\odot/\text{pc}^2$ . The grey-scale is in units of  $M_\odot/\text{pc}^2$ .

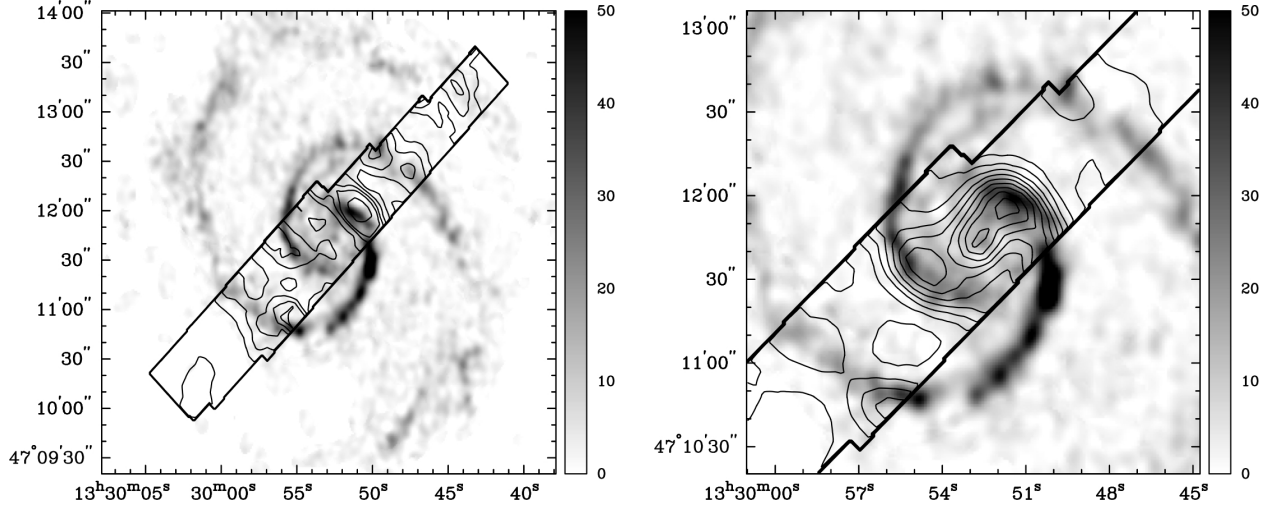


Fig. 7.— *Left:* Comparison of CO intensity (in grey-scale) to the warm ( $T = 100 - 300$  K) H<sub>2</sub> mass (in contours). The CO intensity is in units of Jy beam s<sup>-1</sup>. The warm H<sub>2</sub> mass contours are the same as in Figures 3 and 4. *Right:* Comparison of CO intensity (in grey-scale) to the hot ( $T = 400 - 1000$  K) H<sub>2</sub> mass (in contours). The CO intensity is in units of Jy beam s<sup>-1</sup>. The hot H<sub>2</sub> mass contours are the same as in Figures 3 and 5.

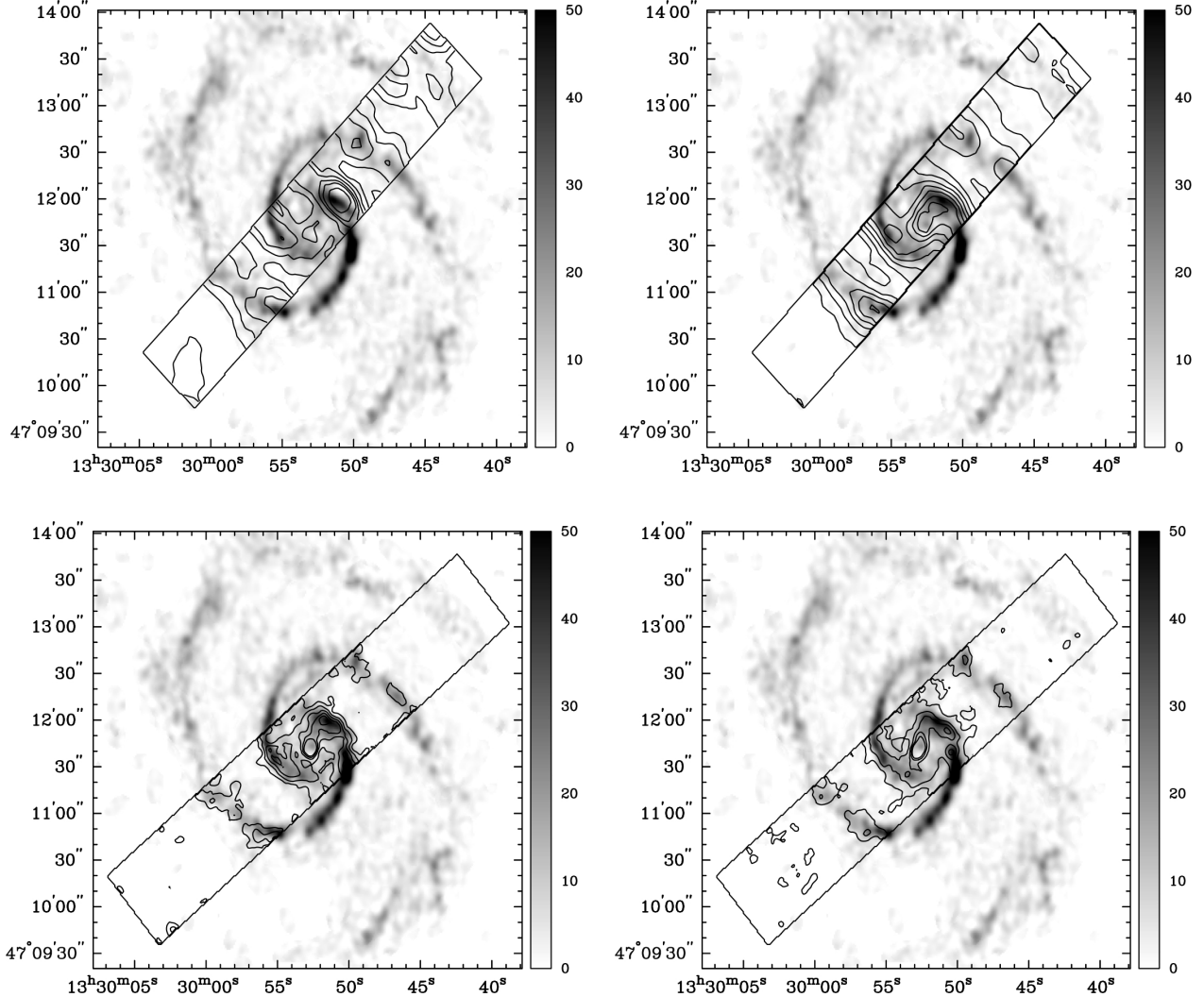


Fig. 8.— Comparison of the CO emission to the H<sub>2</sub> S(0) (*top left*), H<sub>2</sub> S(1) (*top right*), H<sub>2</sub> S(2) (*bottom left*), and H<sub>2</sub> S(3) (*bottom right*) emission. The CO emission maps are in units of Jy beam s<sup>-1</sup>. Contour levels for H<sub>2</sub> S(0), H<sub>2</sub> S(1), H<sub>2</sub> S(2), and H<sub>2</sub> S(3) are the same as in Figure 1.

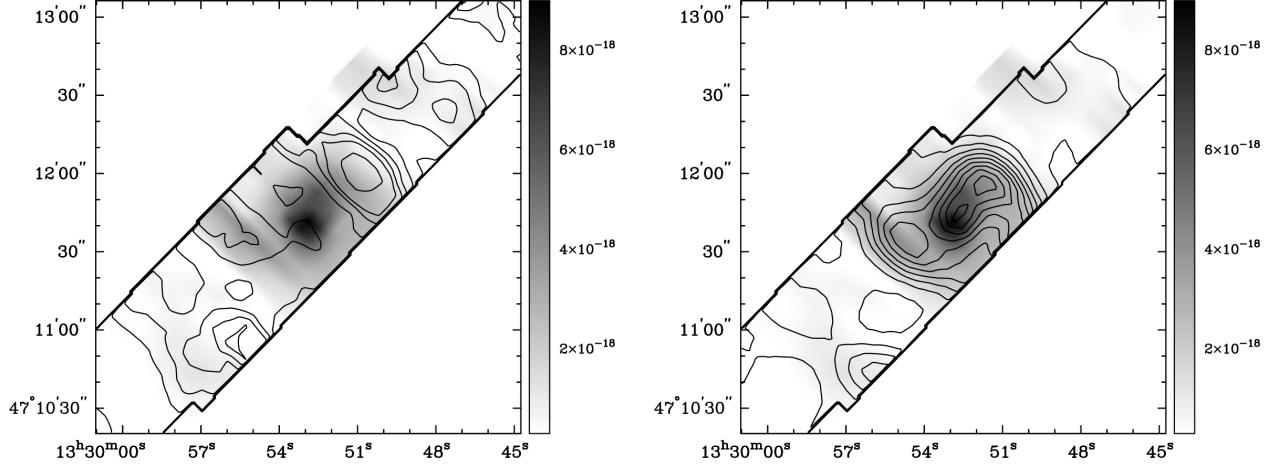


Fig. 9.— *Left:* Comparison of the [O IV](25.89  $\mu\text{m}$ ) emission (in grey-scale) to the warm ( $T = 100$  K - 300 K)  $\text{H}_2$  mass distribution (in contours). Hot  $\text{H}_2$  mass contours are the same as in Figures 3 and 4. *Right:* Comparison of the [O IV](25.89  $\mu\text{m}$ ) emission (in grey-scale) to the hot ( $T = 400$  - 1000 K)  $\text{H}_2$  mass distribution (in contours). Hot  $\text{H}_2$  mass contours are the same as in Figures 3 and 5. The [O IV](25.89  $\mu\text{m}$ ) emission is in units of  $\text{W}/\text{m}^2$ .

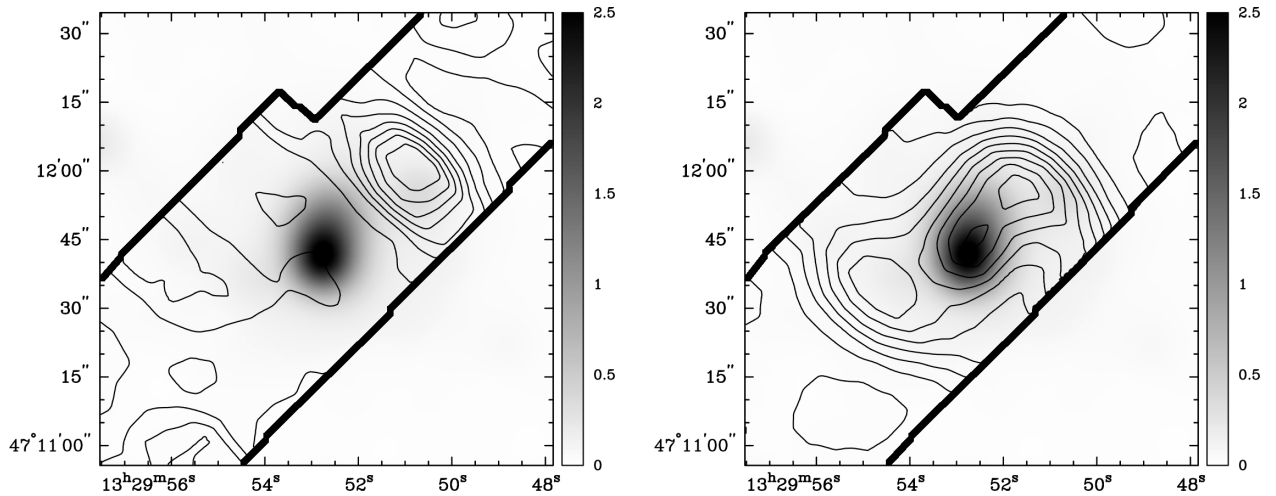


Fig. 10.— *Left:* Comparison of the smoothed 0.5 - 10 keV X-ray emission band (in grey-scale) to the warm ( $T = 100 - 300$  K) H<sub>2</sub> mass distribution (in contours). The X-ray image has been smoothed to the same resolution as the warm H<sub>2</sub> mass map, 10''.2. X-ray emission is in units of counts. H<sub>2</sub> mass contours are the same as in Figures 3 and 4. *Right:* Comparison of the smoothed 0.5 - 10 keV X-ray emission band (in grey-scale) to the hot ( $T = 400 - 1000$  K) H<sub>2</sub> mass distribution (in contours). The H<sub>2</sub> mass distribution contours are the same as in Figures 3 and 5.

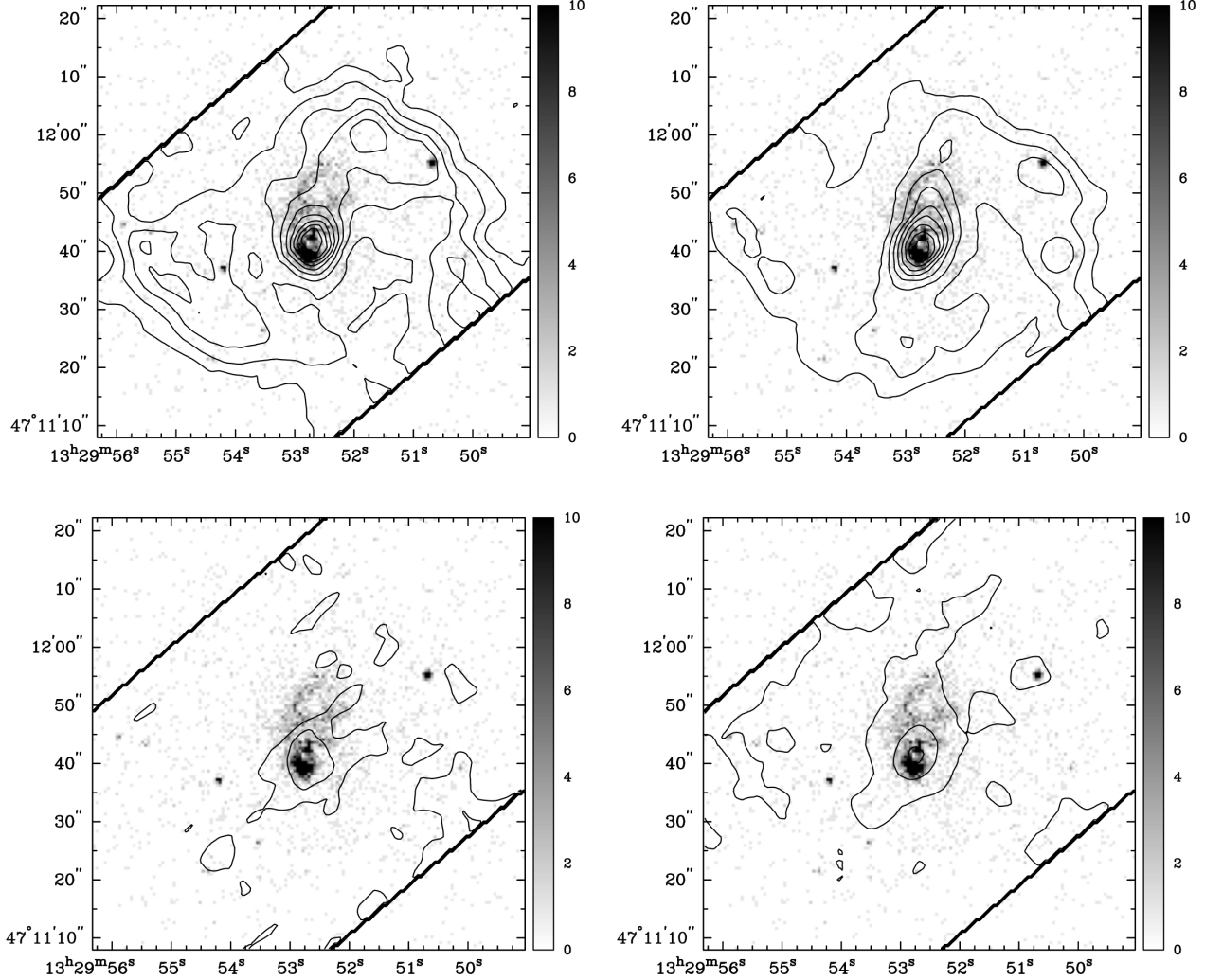


Fig. 11.— Comparison of the 0.5 - 10 keV X-ray emission band (in grey-scale) to the H<sub>2</sub> S(2) (*top left*), H<sub>2</sub> S(3) (*top right*), H<sub>2</sub> S(4) (*bottom left*), and H<sub>2</sub> S(5) (*bottom right*) emission in the nuclear region of NGC 5194. X-ray emission is in units of counts. The H<sub>2</sub> S(2) and H<sub>2</sub> S(3) emission contours are at 10 % of their peak values ( $2.20 \times 10^{-18}$  and  $1.35 \times 10^{-17}$  W/m<sup>2</sup>, respectively). The H<sub>2</sub> S(4) contours are at  $2.0 \times 10^{-18}$  and  $1.0 \times 10^{-18}$  W/m<sup>2</sup> and the H<sub>2</sub> S(5) contours are at  $7.3 \times 10^{-18}$ ,  $4.0 \times 10^{-18}$ , and  $8.0 \times 10^{-19}$  W/m<sup>2</sup>.

Table 1. Resolution of the H<sub>2</sub> Maps

Transition	Wavelength ( $\mu\text{m}$ )	Spatial Resolution	$\lambda/\delta\lambda$
H <sub>2</sub> (0-0)S(0)	28.22	10''2	155
H <sub>2</sub> (0-0)S(1)	17.04	6''17	185
H <sub>2</sub> (0-0)S(2)	12.28	4''37	198
H <sub>2</sub> (0-0)S(3)	9.66	3''44	156
H <sub>2</sub> (0-0)S(4)	8.03	2''85	129
H <sub>2</sub> (0-0)S(5)	6.91	2''46	223

Table 2. H<sub>2</sub> Parameters

Transition	Wavelength ( $\mu\text{m}$ )	Rotational State (J)	Energy (E/k)	A ( $\text{s}^{-1}$ )	Statistical Weight (g)
H <sub>2</sub> (0-0)S(0)	28.22	2	510	$2.94 \times 10^{-11}$	5
H <sub>2</sub> (0-0)S(1)	17.04	3	1015	$4.76 \times 10^{-10}$	21
H <sub>2</sub> (0-0)S(2)	12.28	4	1682	$2.76 \times 10^{-9}$	9
H <sub>2</sub> (0-0)S(3)	9.66	5	2504	$9.84 \times 10^{-9}$	33
H <sub>2</sub> (0-0)S(4)	8.03	6	3474	$2.64 \times 10^{-8}$	13
H <sub>2</sub> (0-0)S(5)	6.91	7	4586	$5.88 \times 10^{-8}$	45
H <sub>2</sub> (0-0)S(6)	6.11	8	5829	$1.14 \times 10^{-7}$	17
H <sub>2</sub> (0-0)S(7)	5.51	9	7197	$2.00 \times 10^{-7}$	57

Note. — The statistical weight (g) is  $(2J+1)(2I+1)$  where  $I$  equals 1 for odd J transitions (ortho transitions) and  $I$  equals 0 for even J transitions (para transitions).